Latin American Journal of Solids and Structures
www.lajss.org

Study of the anti-penetration performance of concrete with different coarse aggregate content

Abstract

Deep penetration experiments were performed on five types of concrete with different coarse aggregate content. The projectile diameter was 29.9 mm, the initial velocity was 647 m/s, and the volume fraction of the coarse aggregate was between 0% and 59.0%. The damage laws and damage mechanism of the target were analyzed. The pure mortar target had the smallest radial crack origin diameter and crater depth. Too high of the coarse aggregate content led to the formation of many voids, which led to the disappearance of radial cracks, crater surface bypassing the coarse aggregate and a large reduction of crater diameter. The influence laws and mechanism of the coarse aggregate on the penetration depth were also analyzed. The increase of volume fraction of coarse aggregate was beneficial to reducing penetration depth and the increase of voids volume fraction was opposite. The penetration depth was the lowest when the volume fraction of the coarse aggregate reached the maximum and no voids formed. By modifying the static resistance stress in the Forrestal penetration formula, a penetration depth model considering the volume fractions of the coarse aggregate and voids was established. The predicted results were in good agreement with the experimental results.

Keywords

Projectile penetration; Concrete; Coarse aggregate; Mesoscale

Cheng Wu[a]
Wenbin Li[a]*
Xiaojun Shen[b]

[a] Ministerial Key Laboratory of ZNDY, Nanjing University of Science and Technology, Nanjing, China. E-mail: qqqwucheng@163.com, lwb2000cn@njust.edu.cn

[b] Beijing Special Electrical and Mechanical Research Institute, Beijing, China. E-mail: SXJ_1959@126.com

* Corresponding author

http://dx.doi.org/10.1590/1679-78255072

Received: May 10, 2018
In Revised Form: May 28, 2018
Accepted: May 30, 2018
Available Online: May 30, 2018

1 INTRODUCTION

Concrete is widely used in military and civil fields, such as the subterranean command centers, nuclear reactor containments, bridges and dams. Its anti-penetration performance has been studied extensively for a long time (Mumma and Randall, 1977; Forrestal and Tzou, 1997; Zhang et al., 2017). Because the composition and mechanical properties of concrete are complicated, the anti-penetration performance is very difficult to accurately predict (Yankelevsky, 2017). Using environment, construction conditions and cost have different requirements on concrete mix proportion, leading to considerable differences in the volume fraction of coarse aggregate. For example, the volume fraction of the coarse aggregate of self-compacting concrete is approximately 30%, that of ordinary concrete is approximately 40~50%, and that of four-graded concrete is approximately 60~70%. Therefore, studying the influence of the coarse aggregate content on the damage and penetration depth of concrete is necessary.

The influence of aggregate on penetration has been mainly studied by experimentation and numerical simulation. In the aspect of experimentation, Zhang et al. (2005), Wang et al. (2016) and Wu et al. (2015a) studied the crater and penetration depth with different strength concrete. The high strength concrete, which was obtained by excluding coarse aggregate, could not reduce the penetration depth; however, the other variables, such as the water cement ratio and reinforcement ratio, were not unified. Zhang et al. (2012) studied the influence of the coarse aggregate size on the crater diameter and penetration depth, and the penetration depth was less than 7 times of the projectile diameter. The effects of the coarse and fine aggregate types on the nose abrasion and penetration depth of projectile were studied by Wu et al. (2012) and Yang (2015), respectively. Bludau et al. (2006) studied the effects of the aggregate type, maximum aggregate size, cementitious material content and gradation curve on the front and rear face crater volume of thin target. The effect of the maximum aggregate size on the penetration resistance and the fragments size distribution of thin target were studied by Werner et al. (2013). Dancygier et al. (2007) studied the effects of maximum coarse aggregate size and type on the perforation limit and front and rear face crater diameter of thin target. Dancygier et al. (2014) studied the effect of maximum coarse aggregate size on the damage and penetration resistance of double layer thin target. Wu et al. (2015b) studied the influence of the corundum aggregate size and volume fraction on the crater area and penetration depth at impact speed of 510 m/s; the coarse aggregate volume fractions were 30% and 45%, and the penetration depth was less

than 6 times the projectile diameter. In the aspect of numerical simulation, Wriggers and Moftah (2006) and Zhou and Hao (2009) provided the method to establish a mesoscale geometric model of concrete. Fang and Zhang (2014) and Deng et al. (2017) studied the effect of coarse aggregate on the projectile deflection. Zhang et al. (2014) studied the effect of the aggregate type on the projectile perforation velocity. The current experimental study about the effects of coarse aggregate content on penetration focuses on thin target perforation and shallow penetration, and is lack of deep penetration research. At the same time, coarse aggregate content needs to be further increase. Moreover, it is necessary to elucidate the influencing mechanism of coarse aggregate and develop a theoretical penetration depth model that considers the coarse aggregate content.

In this paper, penetration experiments of ogive-head long-rod projectile penetrating into concrete with different coarse aggregate content were performed. The initial velocity of the projectile was 647 m/s. The minimum coarse aggregate content was 0; and at the maximum content, the coarse aggregates contacted with each other and created voids. The damage law and mechanism of the radial cracks and crater of the target were studied. The law and mechanism of the influence of the coarse aggregate content on the penetration depth were also analyzed. Based on the Forrestal penetration theory, a theoretical model of the penetration depth, considering the volume fractions of the coarse aggregate and voids, was developed and compared with both the commonly used penetration formula and experimental results.

2 Penetration experiment

2.1 Projectile

The projectile (Fig. 1) consisted of solid projectile body and obturator ring with a total mass of 0.976 kg. The mass of the obturator ring was 0.0072 kg. The projectile diameter was 0.0299 m, the ratio of the projectile length to diameter was 7, the caliber-radius-head was 4, material was 35CrMnSiA, and Rockwell hardness was 44. The obturator ring was connected to the projectile body by thread, and material was monomer casting (MC) nylon.

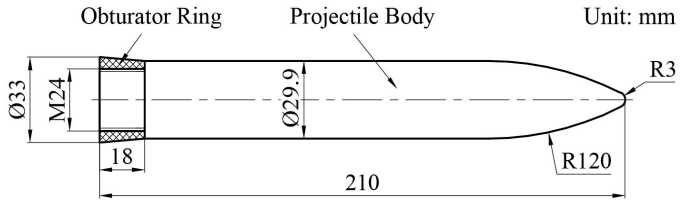

Figure 1: *Structure and size of projectile*

2.2 Concrete target

Mix proportion. The concrete mix proportion and basic performance parameters are given in Table 1. The strength grade of cement was 32.5R. The fine aggregate was quartz sand. The coarse aggregate was crushed limestone; the maximum size of the coarse aggregate was 31.5 mm, and the packing volume fraction was 59.0%. Coarse aggregate content refers to the relative content of coarse aggregate in mass mix proportion. The mix proportions of the mortar in concretes c1~c5 were consistent, while the content of the coarse aggregate gradually increased from c1 to c5. The cross section diagram is shown in Fig. 2.

Table 1: *Concrete mix proportion and basic performance parameters*

Concrete number	Mass mix proportion				Volume fraction (%)			Calculated density (kg/m^3)	150 mm cube density (kg/m^3)	Uniaxial compressive strength f_{c150} (MPa)
	Cement	Water	Fine aggregate	Coarse aggregate	Mortar λ_s	Coarse aggregate λ_g	Voids λ_j			
c1	1	0.4	1.45	0	100	0	0	-	2114	38
c2				0.933	79.7	20.3	0	2235	2212	40
c3				2.49	59.5	40.5	0	2356	2367	45
c4				5.60	38.5	59.0	2.5	2414	2423	42
c5				14.9	14.5	59.0	26.5	1907	2044	7.0

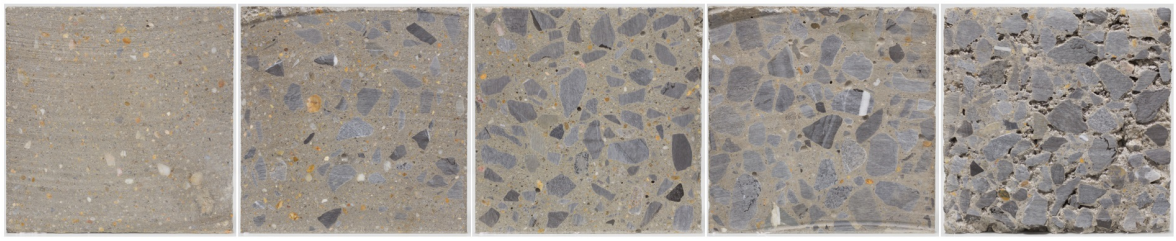

Figure 2: *Cross section of the 150 mm cube specimens with volume fraction of mortar 100%, 79.7%, 59.5%, 38.5 and 14.5%, respectively*

Coarse aggregate density. The saturated density of the crushed limestone was measured by density cup and electronic scale. The saturated density was 2714 kg/m^3, the natural dry density of the limestone was 2712 kg/m^3, and the density was 2709 kg/m^3 after drying at 110°C.

Volume fractions of the mortar, coarse aggregate and voids. The volume fraction was calculated by the mass mix proportion, mortar density, natural dry density and packing volume fraction of the crushed stone. The mortar was simplified as a homogeneous material, and the pore structure in the mortar was ignored. The coarse aggregate was surrounded by mortar in the c1~c3, which had voids volume fraction of 0. The coarse aggregates in the c4 and c5 were in contact with each other, and the volume fraction of the coarse aggregate reached the maximum, approximately equaled to the packing volume fraction 59.0%. In these concretes, the mortar could not completely fill the voids between the coarse aggregates, resulting in air voids. As the mortar volume fraction was an independent variable that determined the volume fractions of the coarse aggregate and voids, the mortar volume fraction was used as the variable in this paper.

Calculated density of the concrete. The calculated density was calculated by using the volume fraction, mortar density and natural dry density of the limestone. For c2~c4, the calculated density was approximately equal to the 150 mm cube density. For c5, the density of the 150 mm cube was 7.2% higher than the calculated value because the concrete was difficult to stir evenly. Therefore, the calculated density was more representative of the average density of large volume target.

Uniaxial compressive strength. The uniaxial compressive strengths of the concretes were tested by 150 mm cubes (Fig. 3), approximately 4 months from the pouring date. By force control, the loading rate was 15 kN/s. The uniaxial compressive strengths of c1~c4 varied by 18%. For c5, the voids resulted in a decrease of 83% in the uniaxial compression strength, compared to c4.

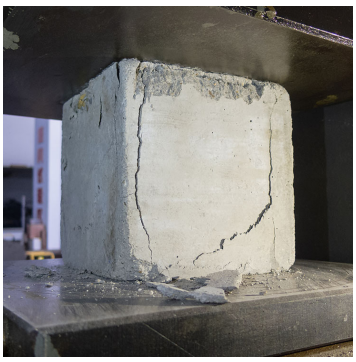

Figure 3: *Uniaxial compression test*

Figure 4: *Structure and size of target*

Target. The target consisted of concrete, steel hoop and cliver (Fig. 4). The target diameter was 0.9 m, and the target length was between 1.45 and 1.50 m. The concrete target and the 150 mm cube were poured in the same batch, and the penetration test was performed approximately 3 months after pouring. The target number corresponds to the concrete number; for example, the targets c1-1~c1-4 correspond to the concrete c1.

2.3 Experimental scheme

The Experimental layout is shown in Fig. 5. During the experiments, the projectiles were launched through a 30 mm smoothbore gun. The appropriate propellant was chosen to burn completely in the bore, which could reduce the instability of the initial velocity, and avoid the image overexposure by the high speed camera. The distance between the gun muzzle and the target has a significant effect on the experiment; if the distance is too small, it cannot meet the requirements of velocity measurement; if the distance is too large, the projectile will gradually appear an attack angle (the projectile does not have rotation stability and tail stability). After adjusting, the distance between the gun muzzle and the target was determined to be 3m. The projectile initial velocity of projectile was measured using a high speed camera, and calibrated the ballistic line using calibration rod before the experiment. To ensure that the projectile image was clear, the projectile was sprayed with a layer of black paint and a white background was arranged before launching. A projectile receiver, containing a sand pile inside, was located behind the target to ensure the safety of the test.

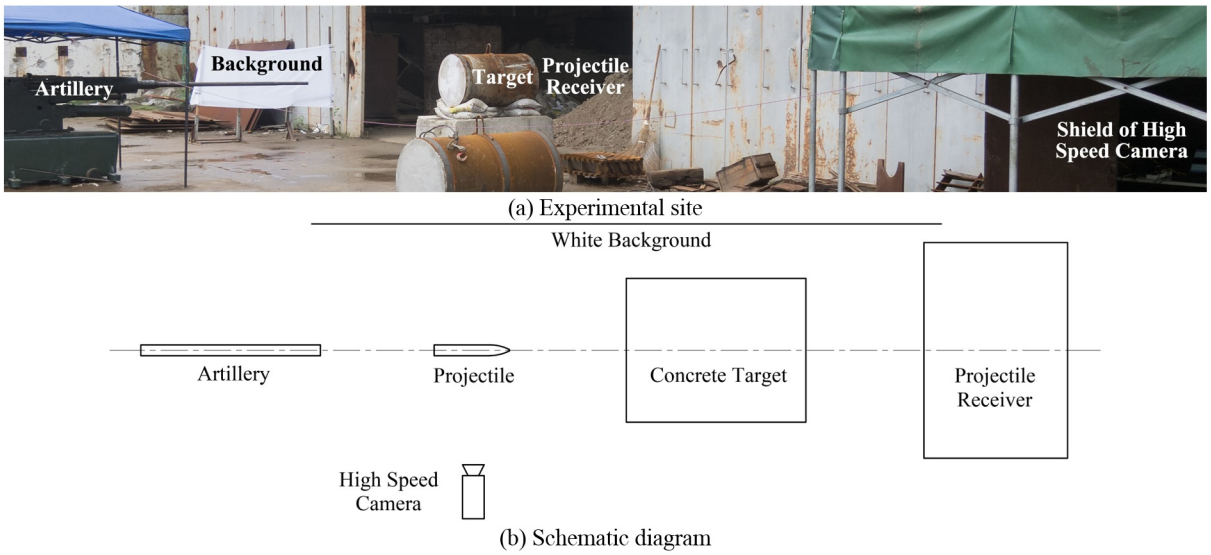

Figure 5: *Experimental layout*

In this paper, deep penetration tests were performed for five different concretes. Considering that the voids in c5 would greatly reduce the penetration resistance, if c5 was guaranteed not to be perforated, it was very difficult for the other targets to reach deep penetration at the same initial velocity. For c1~c4, because c1 had no coarse aggregate, its penetration resistance was predicted to be relatively low. Therefore, the compromise scheme was to make the projectile penetrate into c1 as deeply as possible, and rear face scabbing not occur. First, the penetration test of c1-3 was performed. The projectile stopped in the shallow layer of the sand pile in the projectile receiver, so the residual velocity of the projectile was approximately 0. The projectile initial velocity was reduced to penetrate c1-4, and no scabbing formed on the back of the target. Therefore, the rest of the tests used the same projectile initial velocity.

2.4 Experimental results

After penetration, the projectile was recovered from the target. The nose abrasion was negligible, and the obturator ring was compressed but not removed, as shown in Fig. 6.

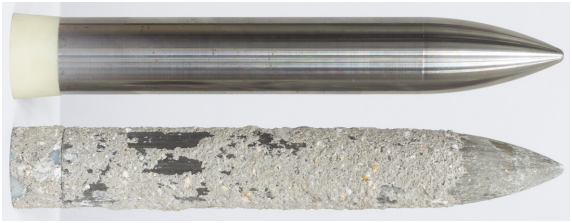

Figure 6: *Unfired and recovered projectiles*

Table 2 shows the damage and penetration depth of five types of concrete targets. The trajectory deflection of c1~c4 was negligible. For c5-1~c5-3, the ballistic deflection was caused by the uneven of targets, and the trajectory end point deviated from the impact point by 9.3°, 7.9° and 10.7°, respectively. The projectile perforated the 1.50m thick target c5-1, and flew upward at an angle of 20° with incidence direction, with residual velocity of V_r=380 m/s. The residual velocity of c5-2 and c5-3 failed to measure.

Table 2: *Target damage and penetration depth*

Target number	Initial velocity V_0 (m/s)	Radial crack origin diameter D_0 (m)	Maximum crater diameter D_1 (m)	Minimum crater diameter D_2 (m)	Crater depth h_c (m)	Penetration depth P (m)	Remark
c1-3	736	0.14	0.41	0.34	0.068	-	Perforation
c1-2	641	0.14	0.39	0.36	0.086	1.03	-
c1-4	649	0.13	0.47	0.40	0.062	1.12	-
c2-1	647	0.17	0.43	0.41	0.094	0.761	-
c2-2	653	0.16	0.40	0.31	0.097	0.776	-
c2-3	650	0.18	0.40	0.33	0.10	0.701	-
c3-2	653	0.16	0.39	0.32	0.12	0.659	Coring before test
c3-3	650	0.14	0.47	0.38	0.096	0.702	-
c3-4	653	0.17	0.43	0.30	0.10	0.704	-
c4-1	651	0.17	0.49	0.38	0.10	0.597	-
c4-2	653	0.14	0.46	0.39	0.11	0.653	-
c4-3	647	0.15	0.55	0.39	0.10	0.667	-
c5-1	640	-	0.29	0.25	0.12	-	Perforation
c5-2	647	-	0.25	0.24	0.10	-	Perforation
c5-3	640	-	0.38	0.27	0.11	-	Perforation

3 Target damage analysis

3.1 Radial crack

Fig. 7 shows the front surface damage of the 5 types of concrete targets. Radial cracks were produced under tensile stress at the surface of c1~c4 and extended to the edge of the target. The numerous voids in concrete c5 attenuated the propagation of the wave, thereby reducing the range of the radial damage of the target, and no radial crack was observed on the target surface. Therefore, c5 was suitable for resisting multiple penetrations and absorbing shock wave.

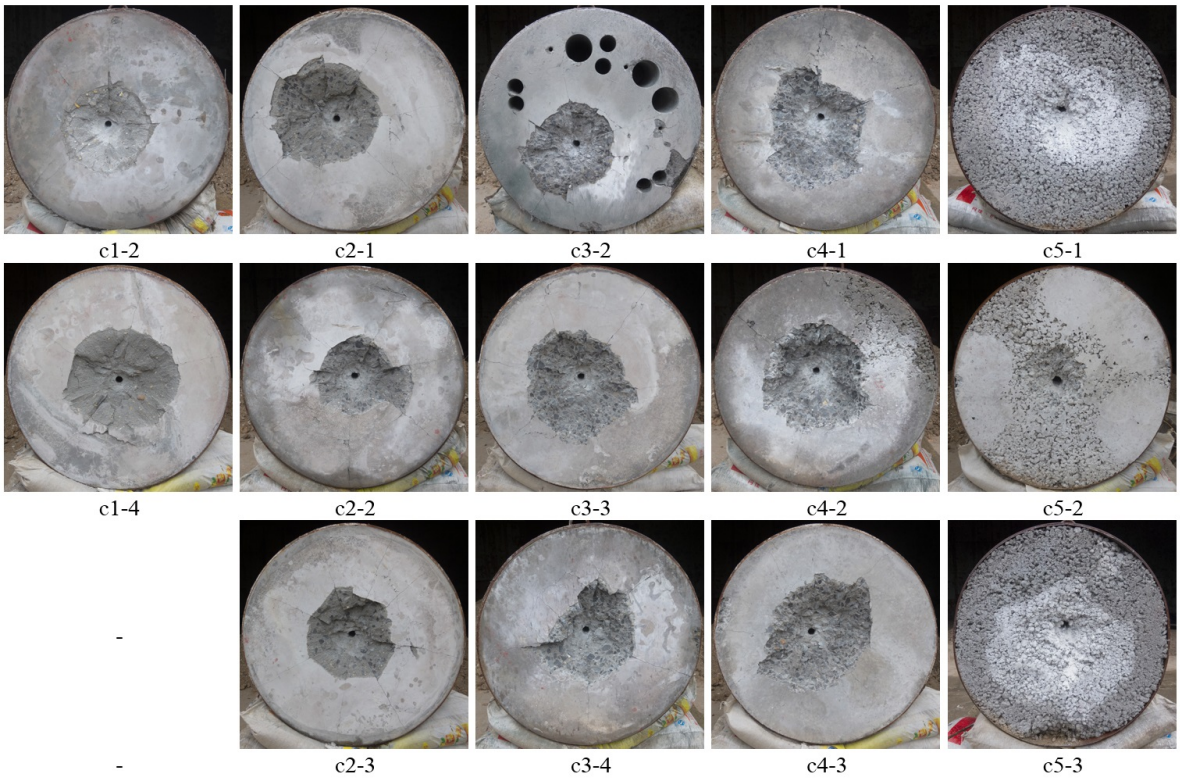

Figure 7: *Image of the font surface damage of the target with volume fraction of mortar 100%, 79.7%, 59.5%, 38.5 and 14.5%, respectively*

The local magnification images of the typical targets are shown in Fig. 8. C1~c4 were divided into two areas by the radial crack origin diameter: a plastic zone in the inner area and a brittle zone in the outer area. The dimensionless radial crack origin diameter D_0/d of c1~c4 is shown in Fig. 9; the average D_0/d of c1 was 15.6% smaller than those of c2~c4. The high compressibility of c1 reduced the propagation of the plastic wave, and correspondingly the size of plastic zone decreased. C3 and c4 had more coarse aggregate than that in c2, reducing their compressibility. However, higher coarse aggregate content increased the absorption of the deformation energy, leading to overall identical size of the plastic zone of c2~c4. The trajectory center of c5 collapsed after compression, and the interior of the trajectory was blocked by falling coarse aggregate and mortar. Because c5 had no radial cracks, it was difficult to identify the boundary of the loose zone.

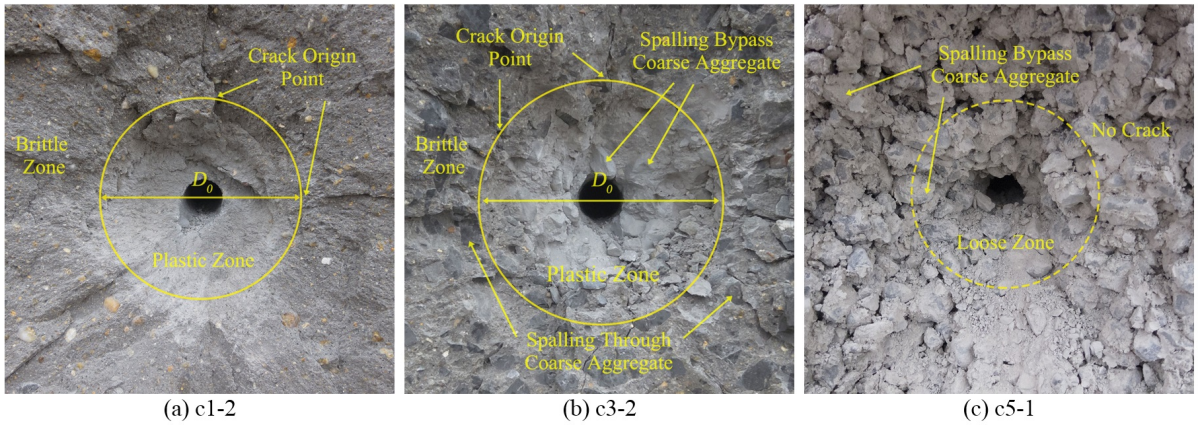

(a) c1-2 (b) c3-2 (c) c5-1

Figure 8: *Local magnification of the crater with volume fraction of mortar 100%, 59.5% and 14.5%, respectively*

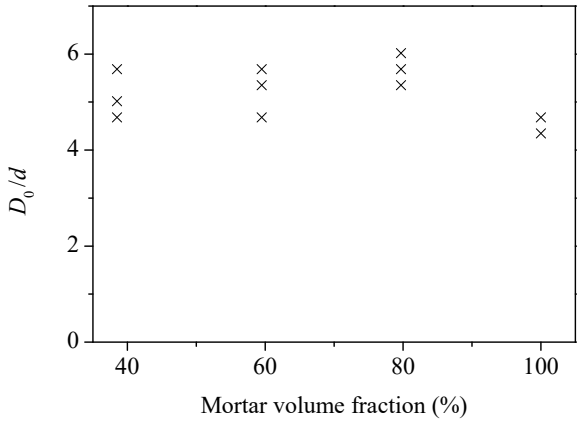

Figure 9: *Dimensionless radial crack origin diameter*

3.2 Crater surface

For the plastic crater zone of c2~c4, the difference of the strain between the coarse aggregate and the mortar was too large, which led to coarse aggregate peeling, then crater surface bypassed the coarse aggregate (Fig. 8b). Under static load for normal strength concrete, the cracks only partially propagated through the coarse aggregate. However, at high strain rate, the brittle crater zone of c2~c4 was mostly propagated through coarse aggregate (Fig. 8b). There was too little mortar in c5, because of weak combination of mortar and coarse aggregate, the crater surface bypassed all the coarse aggregate (Fig. 8c).

3.3 Crater diameter

The crater had a certain asymmetry (Fig. 7), but could be approximated as circular. The dimensionless crater diameter $D_{eq}/d = \sqrt{D_1 D_2}/d$ of c1~c4 was overall identical (Fig. 10). The voids in c5 led to a smaller dimensionless crater diameter; the average D_{eq}/d of c5 was 30.4% lower than those of c1~c4.

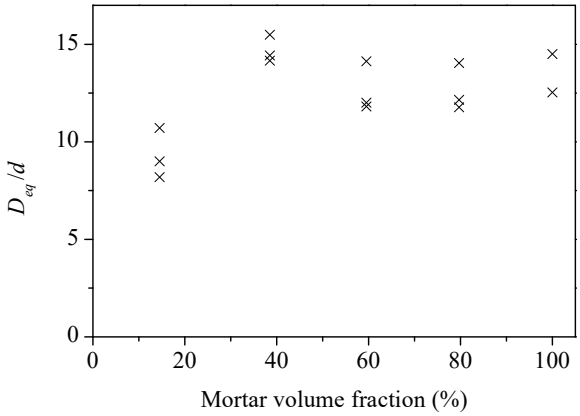

Figure 10: *Dimensionless crater diameter*

3.4 Crater depth

The dimensionless crater depth h_c/d is shown in Fig. 11. The crater depth of c1 was small and had an average of 74 mm. The crater depth of c2~c5 was overall identical and had an average of 104 mm. This difference of 30 mm was approximately the maximum coarse aggregate diameter of 31.5 mm, which was caused by spalling of the coarse aggregate in the center of c2~c5. Therefore, reducing the maximum coarse aggregate diameter helped to reduce the crater depth.

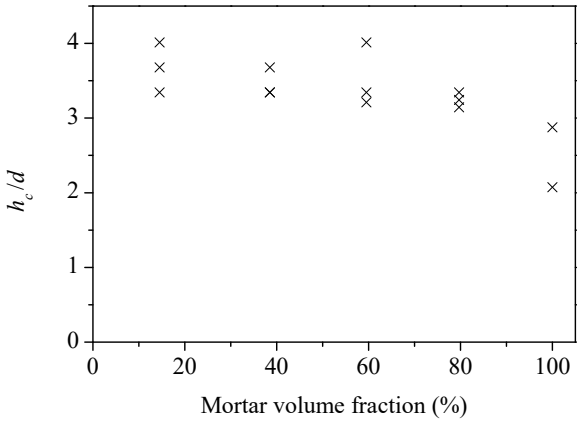

Figure 11: *Dimensionless crater depth*

4 Penetration depth theory

4.1 Modification of the penetration depth test data

The penetration depth of the projectile is shown in Fig. 12. Compared with the crater law, the penetration depth changed only slightly under the same condition and the influence regularity of coarse aggregate was stronger. In deep penetration, the penetration resistance mainly depended on the plastic properties of the concrete under high pressure, which was more stable relative to the brittle properties of the crater. In addition, the projectile nose acted on a considerable amount of coarse aggregate during deep penetration, thus reducing the randomness.

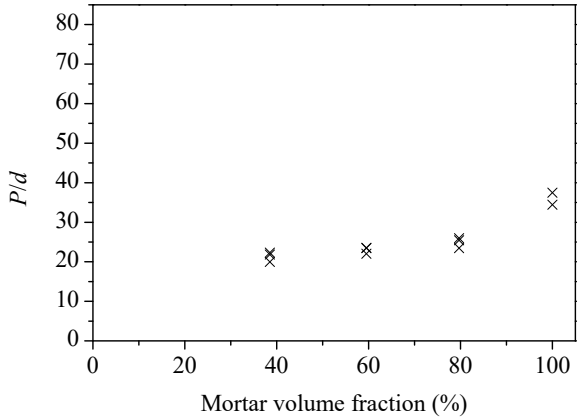

Figure 12: *Dimensionless penetration depth*

Because the c5 target was perforated, its penetration depth could not be directly compared with the other targets. Table 2 shows that under the same propellant weight, the initial velocity of the projectile was 640~653 m/s, and the variability in the kinetic energy was 4.1%. To compare the penetration depth of c1~c5 and to ensure the same initial velocity of the projectile, the penetration depth should be modified. After the crater stage, the deceleration of a rigid ogive-nose projectile penetrating into a semi-infinite concrete target at medium speed approaches a constant (Rosenberg and Dekel, 2010; Frew et al., 2006). For deep penetration, the penetration depth is approximately proportional to the square of the velocity. Based on the initial velocity of the projectile at 647 m/s, the modified penetration depth P_{647} is

$$P_{647} = \frac{647^2}{V_0^2 - V_r^2} P \tag{1}$$

Fig. 13 shows the dimensionless penetration depth P_{647}/d of the five types of concrete. With an increase in the volume fraction of the mortar, the dimensionless penetration depth first decreased and then increased. Because the mortar had a lower deformation resistance to the projectile relative to coarse aggregate, too much mortar increased the penetration depth. For example, c1 increased by 70.9% relative to c4. However, too low of the volume fraction of mortar would

result in the inability of the mortar to completely fill the voids between the coarse aggregate, increasing the overall compressibility of the concrete. In addition, the mechanical properties of the geo-material are enhanced with confining pressure, and the voids reduced the confining pressure of the coarse aggregate and mortar, thus reducing the flow shear stress of the concrete. Therefore, the presence of many voids would lead to a significant increase in the penetration depth; for example, the penetration depth of c5 increased by 274% relative to c4. The penetration resistance of c4 was the greatest; however, because of the low mortar content, the fluidity of c4 was poor, and it was difficult to vibrate evenly during pouring. The average penetration depth of c3 was 7.2% higher than that of c4, but the c3 concrete had good fluidity and was easy to fabricate.

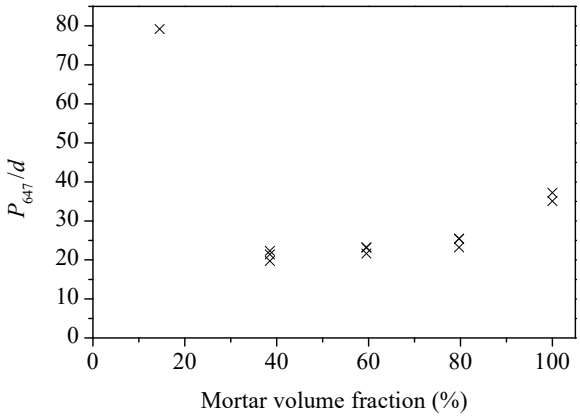

Figure 13: *Modified dimensionless penetration depth*

4.2 Penetration depth theory

4.2.1 Forrestal penetration formula

The Forrestal penetration formula (Forrestal et al., 1994; Frew et al., 1998) had the theoretical foundation of cavity expansion and was calibrated by many experiments; therefore, this formula was widely used. The penetration resistance F and penetration depth are as follows:

$$F = \begin{cases} cz & , \ 0 < z \le 2d \\ \pi d^2 (R + N\rho V^2) / 4 & , \ z > 2d \end{cases} \tag{2}$$

$$R = 1.517 \times 10^5 f_c'^{0.456} \tag{3}$$

$$P = \frac{2m}{\pi N d^2 \rho} \ln[1 + \frac{N(2mV_0^2 - \pi d^3 R)\rho}{(2m + \pi d^3 N\rho)R}] + 2d \tag{4}$$

Here, z is the instantaneous penetration depth. The constant c can be calculated by two resistance equations at $z=2d$. R is the static resistance stress of the concrete. $N=(8\Psi-1)/(24\Psi^2)$ is the nose shape coefficient, where Ψ is the caliber-radius-head. ρ is the concrete density. V is the instantaneous velocity of the projectile. The Eq. (3) is dimensional related, and unit Pa is used.

The Forrestal penetration formula mainly uses the compressive strength of the concrete to predict the penetration resistance characteristics (Eq. (3)), but concretes with the same compressive strength have diverse mix proportions; therefore, the penetration resistance is also significantly different. Modifying the Forrestal penetration formula is necessary to describe the penetration resistance of mesoscale concrete.

4.2.2 Penetration depth model considering the volume fraction of coarse aggregate (Wu et al., in press)

In the author's previous work, numerical simulation of rigid projectile deeply penetrating a mesoscale concrete target was performed. The impact position, coarse aggregate shape, maximum coarse aggregate size, coarse aggregate gradation and coarse aggregate volume fraction were considered. The ratio of maximum coarse aggregate size to the projectile diameter did not exceed 1.5, and the volume fraction of the coarse aggregate was 0~50%. The effects of the impact location, coarse aggregate shape, maximum coarse aggregate size and coarse aggregate gradation on the penetration depth could be ignored, and the volume fraction of the coarse aggregate had a significant effect on the penetration depth.

The local mesh section of the target and projectile is shown in Fig. 14. Part 1 was filled with limestone and part 2 was filled with mortar to represent concrete target; all were filled with mortar to represent pure mortar target; all were filled with limestone to represent rock target. The penetration resistance-time curves for the projectile by part 1 and part 2 were outputted separately. The resistance of part 1 in the rock target was significantly higher than that of part 1 in the concrete target. This result is due to the fact that the strength and stiffness of the coarse aggregate was much greater than that of the mortar which led to limited confining pressure applied by the mortar to the coarse aggregate and as a result significantly reduced the strength of the coarse aggregate. The resistance of part 2 in the concrete target and mortar target were basically the same, which was due to the fact that the mortar was interconnected and easy to compress, so it was less affected by the coarse aggregate.

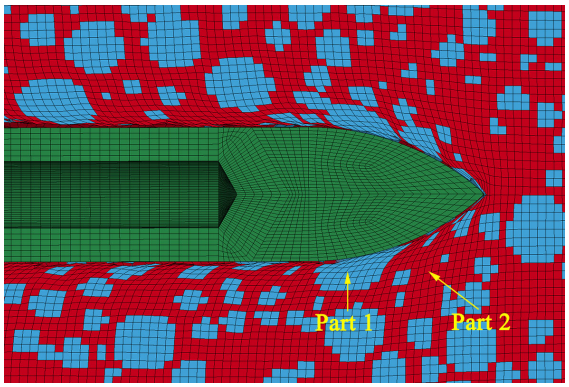

Figure 14: *Local mesh section of the target and projectile*

According to the Forrestal penetration resistance formula, during penetration, the resistance is composed of static resistance $\pi d^2R/4$ and inertial resistance $\pi d^2N\rho V^2/4$. The parameters related to the concrete performance are R and ρ. The volume fraction of the coarse aggregate can be introduced into R. The projectile nose passes through a large amount of mortar and coarse aggregate, so the probability of the contact between the projectile nose and each component is equal to the volume fraction of each component. The mesoscale concrete can be simplified as equivalent homogeneous material with average mechanical properties determined by the linear superposition of the resistance stress of the mortar and coarse aggregate. The static resistance stress R is expressed as

$$R = \lambda_g R_g + \lambda_s R_s \tag{5}$$

where R_g is the coarse aggregate static resistance stress and R_s is the mortar static resistance stress. The stress analysis in this section shows that R_s is an inherent property of the mortar and is not affected by the volume fraction of the coarse aggregate. R_g is affected by the mortar type, but when the mortar type is the same and the volume fraction of the coarse aggregate is different, R_g is constant.

4.2.3 Penetration depth model considering the volume fractions of the coarse aggregate and voids

The volume fraction of the coarse aggregate in the numerical simulation was 0%~50%, and there was no voids between the mortar and coarse aggregate. However, the coarse aggregate content in this paper was higher, which led to the inability of the mortar to completely fill the voids between the coarse aggregates; therefore, the static resistance stress needed to be further modified. When there is no mortar, the coarse aggregates are in contact, and the voids volume fraction is maximized; and as a result the penetration depth is greatly increased. In this situation, it is assumed that the penetration resistance is approximately 0 compared with that without voids. Simplify the effect of voids volume fraction on the decrease of the static resistance stress is linear:

$$R = (\lambda_g R_g + \lambda_s R_s)(1 - \frac{\lambda_j}{\lambda_{j\max}}) \tag{6}$$

Here, $\lambda_{j\max}$ is the maximum voids volume fraction, which mainly depends on the maximum size and gradation of the coarse aggregate; it is 0.41 for the coarse aggregate of this paper.

4.3 Model verification and analysis

The static resistance stress R of the concrete can be calibrated by the test results by using Eq. (4). R_s is calibrated by the penetration result of c1 and is R_s=243.1 MPa. When the volume fraction of the coarse aggregate in concrete is less,

the penetration depth is insensitive to the change in the coarse aggregate static resistance stress R_g, and the calculation precision of R_g is low. Here, the penetration results of the conventional mix proportion c3 are used for the calibration to obtain R_g=655.4 MPa. The static resistance stress of the concrete with different volume fractions of the coarse aggregate and voids can be calculated by Eq. (6).

The R in the Forrestal penetration formula is a function of the uniaxial compressive strength f_c'; where f_c' is measured by testing cylindrical specimens with diameters between 50 and 150 mm and length to diameter ratio of 2. However, in this paper, the uniaxial compressive strength is measured from the 150 mm cube specimen f_{c150}. For ordinary strength concrete, this relationship is approximately f_c'=0.9 f_{c150} (Yi et al., 2006).

The penetration depth is calculated by substituting the static resistance stress calculated by Eq. (6) into Eq. (4) and comparing the results with both the experimental results and commonly used penetration formulas, as shown in Fig. 15. "Experiment" represents the experimental mean value of P_{647}, "Forrestal" represents the results calculated by Eqs. (3) and (4), and "New" is the result of Eqs. (6) and (4). "ACE" and "Modified NDRC" formulas are empirical formulas from experimental statistics (Li et al., 2005). When the coarse aggregate volume fraction is less than 59.0%, an increase in the volume fraction of the coarse aggregate has a limited influence on the compressive strength, while the traditional penetration depth formula mainly uses the compressive strength to characterize the performance of the concrete. Therefore, for c1~c4, the ACE, Modified NDRC and Forrestal formulas cannot reflect the effect of the volume fraction of the coarse aggregate on the penetration depth. The model in this paper can reflect the effect of the volume fraction of the coarse aggregate by considering the concrete component, and the calculated results are in good agreement with the experimental results. For c5, the low mortar volume fraction leads to a significant reduction in the compressive strength, and both the test and the formula show a sharp increase in the penetration depth. For Forrestal, ACE and Modified NDRC formulas, the scope of the application does not include this special concrete, so the prediction error is large. Large volume concrete is difficult to vibrate dense, as a result the actual voids volume fraction is greater than the calculated result. Meanwhile, the model of this paper is linearly simplified, so the predicted results are approximately equivalent to those of the experiment.

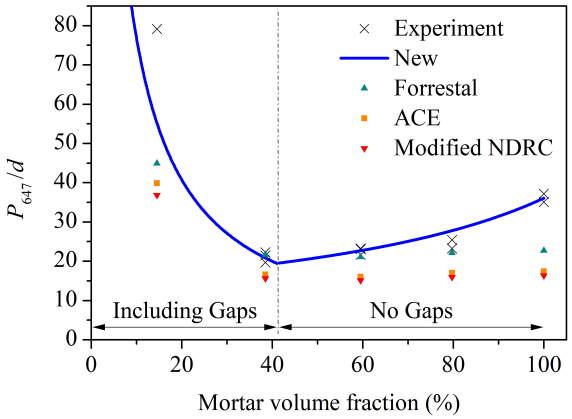

Figure 15: *Comparison of the proposed model with the common penetration formulas and test results*

Fig. 15 shows that too low of the mortar volume fraction produces voids, which result in a significant increase in the penetration depth. When the coarse aggregate volume fraction reaches 59.0% and the voids volume fraction is 0, the penetration depth is the lowest. The maximum value of the coarse aggregate volume fraction can be increased by increasing the maximum coarse aggregate size and optimizing the grading, further increasing the penetration resistance of the concrete.

Fig. 16 shows the influence of volume fraction of the coarse aggregate on penetration depth of rigid projectile at different initial velocities. At the initial velocity of 500 m/s, the penetration depth of pure mortar target is increased by 86.0% compared with that of target with 59.0% volume fraction of the coarse aggregate; at the initial velocity of 1100 m/s, the penetration depth increased by 76.7%. That is, under high initial velocity, the effect of the volume fraction of the coarse aggregate on penetration depth is reduced by 9.3%. The volume fraction of the coarse aggregate mainly affects static resistance and has a limited effect on density in inertial resistance. During high speed penetration, the ratio of inertia resistance increases, and the effect of volume fraction of the coarse aggregate on penetration depth decreases. For a higher penetration speed, the projectile head will be eroded, and the hardness of coarse aggregate has a significant effect on the abrasion of the projectile head (Chen et al., 2010), which is beyond the scope of the theory in this paper and needs further study.

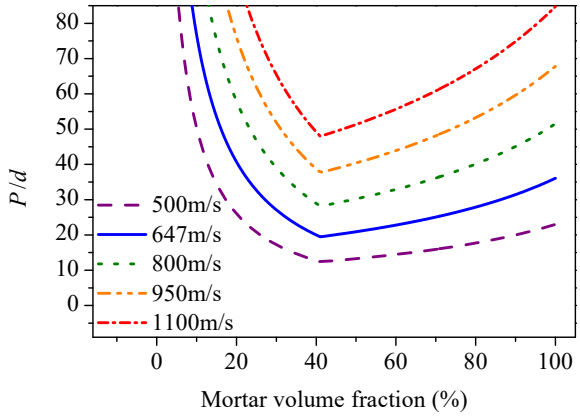

Figure 16: *Dimensionless penetration depth of rigid projectile at different initial velocities* V_0

5 Conclusions

Penetration tests of an ogive-nose long-rod projectile at an initial velocity of 647 m/s penetrating into concrete with different coarse aggregate content were performed, and the following conclusions were obtained:

1. The surface damage and crater laws of five types of concrete were studied. The pure mortar target had the lowest radial crack origin diameter and crater depth. When the voids volume fraction was the highest (when the coarse aggregate content was the highest), the radial crack was not observed, the crater surface bypassed the coarse aggregate, and the crater diameter was greatly reduced.
2. The increase in coarse aggregate volume fraction was beneficial to decrease the penetration depth. Compared with the concrete with coarse aggregate volume fraction of 59.0%, the penetration depth of pure mortar target was increased by 70.9%. The increase of voids volume fraction was opposite, compared with the concrete with 2.5% voids volume fraction, the penetration depth of concrete with 26.5% voids volume fraction was increased by 274%. The penetration depth was the lowest when the volume fraction of coarse aggregate reached the maximum and no voids formed.
3. The stress state of the coarse aggregate and mortar under the penetrating load was analyzed. By modifying the static resistance stress in Forrestal penetration formula, a penetration depth model was established considering the volume fractions of the coarse aggregate and voids. This model was in good agreement with the experimental results.

Acknowledgment

This work was supported by the National Natural Science Foundation of China [grant No. 51278250].

References

Bludau, C., Keuser, M., Kustermann, A. (2006). Perforation Resistance of High-Strength Concrete Panels. Aci Struct J 103(2):188-195.

Chen, X. W., He, L. L., Yang, S. Q. (2010). Modeling on mass abrasion of kinetic energy penetrator. Eur J Mech A-Solid 29(1):7-17.

Dancygier, A. N., Katz, A., Benamou, D., et al. (2014). Resistance of double-layer reinforced HPC barriers to projectile impact. Int J Impact Eng 67(5):39-51.

Dancygier, A. N., Yankelevsky, D. Z., Jaegermann, C. (2007). Response of high performance concrete plates to impact of non-deforming projectiles. Int J Impact Eng 34(11):1768-1779.

Deng, Y. J., Chen, X. W., Yao, Y., et al. (2017). On ballistic trajectory of rigid projectile normal penetration based on a meso-scopic concrete model. Expl Shock Wave 37(3): 377-386. (in Chinese)

Fang, Q. and Zhang, J. (2014). 3D numerical modeling of projectile penetration into rock-rubble overlays accounting for random distribution of rock-rubble. Int J Impact Eng 63(1):118-128.

Forrestal, M. J. and Tzou, D. Y. (1997). A spherical cavity-expansion penetration model for concrete targets. Int J Solids Struct 34(31–32):4127–4146.

Forrestal, M. J., Altman, B. S., Cargile, J. D., et al. (1994). An empirical equation for penetration depth of ogive-nose projectiles into concrete targets. Int J Impact Eng 15(4):395-405.

Frew, D. J., Forrestal, M. J., Cargile, J. D. (2006). The effect of concrete target diameter on projectile deceleration and penetration depth. Int J Impact Eng 32(10):1584-1594.

Frew, D. J., Hanchak, S. J., Green, M. L., et al. (1998). Penetration of concrete targets with ogive-nose steel rods. Int J Impact Eng 21(6):489-497.

Li, Q. M., Reid, S. R., Wen, H. M., et al. (2005). Local impact effects of hard missiles on concrete targets. Int J Impact Eng 32(1):224-284.

Mumma, D. and Randall, D. (1977). Test Results of Earth Penetrators, No. PIFR-865-1. Phys Int Co, California.

Rosenberg, Z. and Dekel, E. (2010). The Deep Penetration of Concrete Targets by Rigid Rods – Revisited. Int J Protective Structures 1(1):125-144.

Wang, S., Le, H. T. N., Poh, L. H., et al. (2016). Resistance of high-performance fiber-reinforced cement composites against high-velocity projectile impact. Int J Impact Eng 95:89-104.

Werner, S., Thienel, K. C., Kustermann, A. (2013). Study of fractured surfaces of concrete caused by projectile impact. Int J Impact Eng 52(52):23-27.

Wriggers, P. and Moftah, S. O. (2006). Mesoscale models for concrete: Homogenisation and damage behavior. Finite Elem Anal Des 42(7):623-636.

Wu, C., Shen, X. J., Wang, X. M., et al. Penetration numerical simulation and penetration depth model of mesoscale concrete target. Expl Shock Wave. (in Chinese, in press, DOI:10.11883/bzycj-2017-0123)

Wu, H. J., Huang, F. L., Wang, Y. N., et al. (2012). Experimental investigation on projectile nose eroding effect of high-velocity penetration into concrete. Acta Armamentarii 33(1):48-55. (in Chinese)

Wu, H., Fang, Q., Chen, X. W., et al. (2015a). Projectile penetration of ultra-high performance cement based composites at 510–1320 m/s. Constr Build Mater 74:188-200.

Wu, H., Fang, Q., Gong, J., et al. (2015b). Projectile impact resistance of corundum aggregated UHP-SFRC. Int J Impact Eng 84:38-53.

Yang, S. (2015). The effect of fine aggregate on the mass loss of high-velocity projectile and its penetration depth, master's thesis, BIT, Beijing. (in Chinese)

Yankelevsky, D. Z. (2017). Resistance of a concrete target to penetration of a rigid projectile – revisited. Int J Impact Eng 106:30-43.

Yi, S. T., Yang, E. I., Choi, J. C. (2006). Effect of specimen sizes, specimen shapes, and placement directions on compressive strength of concrete. Nucl Eng Des 236(2):115-127.

Zhang, M. H., Shim, V. P. W., Lu, G., et al. (2005). Resistance of high-strength concrete to projectile impact. Int J Impact Eng 31(7):825-841.

Zhang, S., Wu, H. J., Zhang, X. X., et al. (2017). High-velocity Penetration of Concrete Targets with Three Types of Projectiles: Experiments and Analysis. Lat Am J Solids Stru 14(9): 1614-1628.

Zhang, W., Mu, Z. C., Xiao, X. K. (2012). Experimental study on effect of aggregate size to anti-penetration ability of concrete targets subjected to high-velocity fragments. Acta Armamentarii 33(8): 1009-1015. (in Chinese)

Zhang, Z. J., Wang, X. M., Li, W. B. (2014). Effect of coarse aggregate type on residual velocity of rigid-projectiles-perforating concrete targets. J VIB Shock 33(7):170-173. (in Chinese)

Zhou, X. Q. and Hao, H. (2009). Mesoscale modelling and analysis of damage and fragmentation of concrete slab under contact detonation. Int J Impact Eng 36(12):1315-1326.